Supporting Information for

Steric hindrance enforced distortion as a general strategy for design of fluorescence "turn-on" cyanide probes

Bin Chen, [a] *Yubin Ding,* [a] *Xin Li,* [b] *Weihong Zhu*, [a] *Jonathan P. Hill,* [c] *Katsuhiko Ariga,* [c] *and Yongshu Xie** [a]

[a]Key Laboratory for Advanced Materials and Institute of Fine Chemicals, East China University of Science and Technology, Meilong 130, Shanghai 200237 (P. R. China). [b]Department of Theoretical Chemistry and Biology, KTH Royal Institute of Technology, SE-10691 Stockholm, Sweden.
[c]WPI-Center for Materials Nanoarchitectonics, National Institute for Materials Science (NIMS), Namiki 1-1, Tsukuba, Ibaraki, Japan.
E-mail: yshxie@ecust.edu.cn

Table of contents

Experimental details

General

Commercially available solvents and reagents were used without further purification. Deuterated solvents for NMR measurements were obtained from Aldrich Chemical Co. Ltd. UV/Vis absorption spectra were measured using a Varian Cary 100 spectrophotometer. Fluorescence spectra were recorded on a Varian Cray Eclipse fluorescence spectrophotometer using a 1cm pathlength quartz cell. Fluorescence lifetime measurements were performed by using the Time Correlated Single Photon Counting (TCSPC) technique following excitation by a nanosecond flash lamp (Edinburgh instruments FL920), and the errors (χ^2) for all the measurements presented were below 1.2. ^{1}H NMR spectra and ^{13}C NMR spectra were obtained using a Bruker AM 400 spectrometer with tetramethylsilane (TMS) as an internal standard. High Resolution Mass spectra (HRMS) were measured on a Waters LCT Premier XE spectrometer. Column chromatography was carried out in air using silica gel (200-300 mesh). **PC2**~**PC5** were prepared according to adaptations of the reported procedures.[1~6] Detection limits[7,8] and fluorescence quantum yields[9~12] of probes **C1~C3** were obtained according to reported methods.

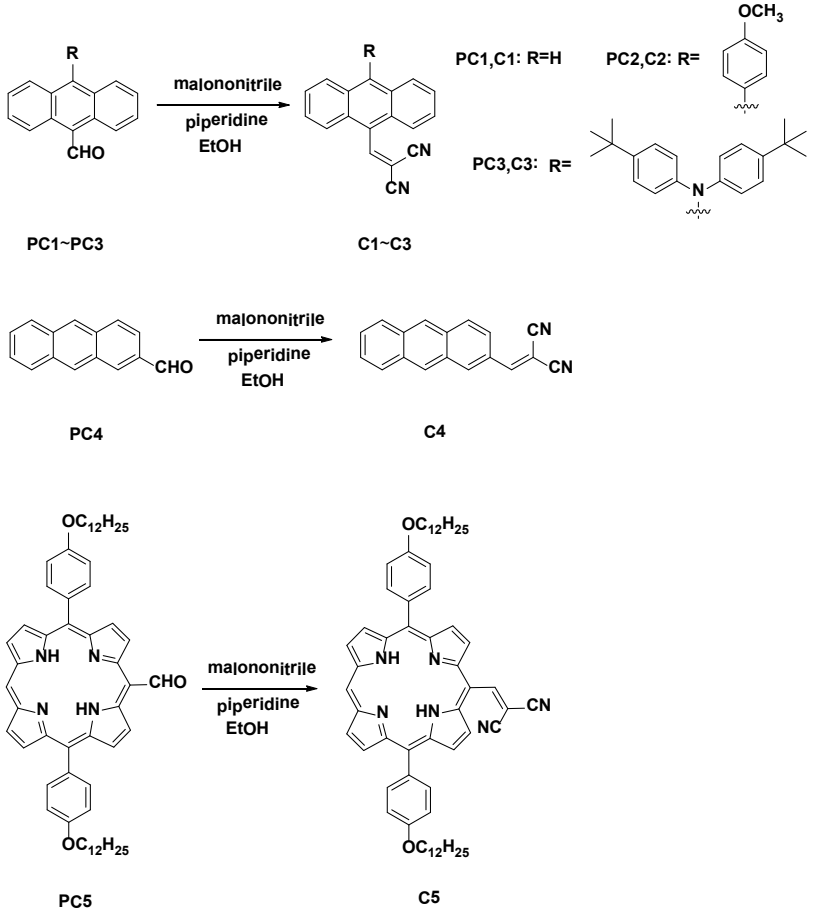

Scheme S1 Syntheses of **C1~C5**.

General procedure for preparation of probes C1~C5

The appropriate formyl substituted precursor (0.2 mmol) and malononitrile (19 μL, 0.3 mmol) were dissolved in a mixed solvent of CH_2Cl_2 (10 mL) and EtOH (10 mL), then piperidine (30 μL, 0.3 mmol) was added. The mixture was stirred at room temperature for 12 h. Then the solvent was removed under reduced pressure and the residue was dissolved in dichloromethane, washed, and

dried over anhydrous sodium sulfate. The product was isolated by chromatography over silica gel then recrystallized from CH_2Cl_2/CH_3OH.

C1.Yield: 49%. ^{1}H NMR ($CDCl_3$, Bruker 400 MHz, 298K): δ 7.56 (t, J = 7.4 Hz, 2H, anthryl), 7.66 (t, J = 7.4 Hz, 2H, anthryl), 7.90 (d, J = 8.8 Hz, 2H, anthryl), 8.07 (d, J = 8.4 Hz, 2H, anthryl), 8.62 (s, 1H, anthryl), 8.90 (s, 1H, -C=CH-). ^{13}C NMR ($CDCl_3$, Bruker 100 MHz, 298K): δ 92.30, 111.43, 113.04, 123.39, 123.90, 126.08, 128.37, 129.10, 129.56, 130.90, 132.55, 160.65. HRMS (ESI, m/z): $[M+H]^+$ calcd for $C_{18}H_{11}N_2$, 255.0922; found, 255.0923.

C2.Yield: 87%. ^{1}H NMR ($CDCl_3$, Bruker 400 MHz, 298K): δ 3.96 (s, 3H, -OCH_3), 7.14 (d, J = 8.4 Hz, 2H, Ph-), 7.33 (d, J = 8.4 Hz, 2H, Ph-), 7.44 (t, J = 7.6 Hz, 2H, anthryl), 7.64 (t, J = 7.6 Hz, 2H, anthryl), 7.80 (d, J = 8.8 Hz, 2H, anthryl), 7.96 (d, J = 8.8 Hz, 2H, anthryl), 9.00 (s, 1H, -C=CH-). ^{13}C NMR ($CDCl_3$, Bruker 100 MHz, 298K): δ 55.47, 92.34, 111.56, 113.13, 114.02, 123.24, 123.94, 125.83, 127.96, 128.48, 128.90, 129.64, 130.11, 131.99, 143.17, 159.50, 161.07. HRMS (ESI, m/z): $[M + H]^+$ calcd for $C_{25}H_{17}N_2O$, 361.1341; found, 361.1344.

C3.Yield: 99%. ^{1}H NMR ($CDCl_3$, Bruker 400 MHz, 298K): δ 1.25 (s, 18H, t-butyl-CH_3), 6.95 (d, J = 8.8 Hz, 4H, Ph-), 7.17 (d, J = 8.4 Hz, 4H, Ph-), 7.45 (t, J = 7.8 Hz, 2H, anthryl), 7.61 (t, J = 7.6 Hz, 2H, anthryl), 7.97 (d, J = 8.8 Hz, 2H, anthryl), 8.24 (d, J = 8.8 Hz, 2H, anthryl) , 8.97 (s, 1H, -C=CH-). ^{13}C NMR ($CDCl_3$, Bruker 100 MHz, 298K): δ 31.39, 34.16, 92.33, 111.51, 113.11, 119.95, 123.23, 124.55, 126.18, 127.09, 128.24, 130.46, 130.51, 143.35, 144.31, 145.09, 160.40. HRMS (ESI, m/z): $[M+H]^+$ calcd for $C_{38}H_{36}N_3$, 534.2909; found, 534.2911.

C4. Yield: 90%. ^{1}H NMR ($CDCl_3$, Bruker 400 MHz, 298K): δ 7.59 (m, 2H, anthryl), 7.91 (s, 1H, anthryl), 8.06 (t, J = 6.6 Hz, 3H, anthryl), 8.10 (s, 1H, -C=CH-), 8.44 (s, 1H, anthryl), 8.47 (s, 1H, anthryl), 8.59 (s, 1H, anthryl). ^{13}C NMR ($CDCl_3$, Bruker 100 MHz, 298K): δ 81.67, 113.05, 114.23, 122.12, 126.70, 126.83, 127.75, 128.32, 128.50, 128.66, 129.83, 130.12, 130.17, 132.26, 132.43, 134.05, 137.06, 159.41. HRMS (ESI, m/z): $[M+H]^+$ calcd for $C_{18}H_{11}N_2$, 255.0922; found, 255.1009.

C5. Yield: 70%. ^{1}H NMR ($CDCl_3$, Bruker 400 MHz), δ: -2.45 (s, 2H, inner NH), 0.91 (t, J = 6.8 Hz, 6H, -CH_3), 1.32 (br, 32H, -CH_2-), 1.62 (m, 4H, -CH_2-), 1.98 (m, 4H, -CH_2-), 4.26 (t, J = 6.4 Hz, 4H, -OCH_2-), 7.31 (d, J = 8.8 Hz, 4H, -Ph), 8.06 (d, J = 8.4 Hz, 4H, -Ph), 8.89 (d, J = 4.4 Hz, 2H, pyrr), 8.99 (d, J = 5.2 Hz, 2H, pyrr), 9.18 (d, J = 4.8 Hz, 2H, pyrr), 9.21 (d, J = 4.8 Hz, 2H, pyrr), 10.10 (s, 1H, meso-H), 10.33 (s, 1H, -CH=C-). HRMS (ESI, m/z): $[M+H]^+$ calcd for $C_{60}H_{71}N_6O_2$, 907.5639; found, 907.5636.

General procedure for preparation of probe-CN adducts

9-Dicyanovinyl anthracene derivatives (0.2 mmol) and tetrabutylammonium cyanide (0.4 mmol) were dissolved in CH_2Cl_2 (40 mL). The reaction mixture was stirred at room temperature for 0.5 h. The mixture was removed under reduced pressure, and the product was isolated by column chromatography over silica gel and recrystallized from CH_2Cl_2/CH_3OH.

C1-CN. Yield: 57%. ^{1}H NMR ($CDCl_3$, Bruker 400 MHz, 298K): δ 4.95 (d, J = 10.8 Hz, 1H, -CH-CN), 6.01 (d, J = 10.8 Hz, 1H, CN-CH-CN), 7.61 (t, J = 7.6 Hz, 2H, anthryl), 7.76 (t, J = 7.8 Hz, 2H, anthryl), 8.15 (d, J = 8.4 Hz, 2H, anthryl), 8.27 (br, 2H, anthryl), 8.69 (s, 1H, anthryl). HRMS (ESI, m/z): $[M - H]^-$ calcd for $C_{19}H_{10}N_3$, 280.0875; found, 280.0878.

C2-CN. Yield: 83%. ^{1}H NMR ($CDCl_3$, Bruker 400 MHz, 298K): δ 3.97 (s, 3H, -OCH_3), 5.03 (d, J = 10.4 Hz, 1H, -CH-CN), 6.11 (d, J = 10.8 Hz, 1H, CN-CH-CN), 7.14 (d, J = 8.4 Hz, 2H, Ph-), 7.32 (d, J = 7.6 Hz, 2H, Ph-), 7.46 (t, J = 7.6 Hz, 2H, anthryl), 7.74 (t, J = 7.6 Hz, 2H, anthryl), 7.84 (d, J = 8.4 Hz, 2H, anthryl), 8.30 (br, 2H, anthryl). HRMS (ESI, m/z): $[M - H]^-$ calcd for

$C_{26}H_{16}N_3O$, 386.1293; found, 386.1295.

C3-CN. Yield: 48%. ^{1}H NMR ($CDCl_3$, Bruker 400 MHz, 298K): δ 1.24 (s, 18H, t-butyl-CH_3), 5.01 (d, J = 10.8 Hz, 1H, -CH-CN), 6.08 (d, J = 10.8 Hz, 1H, CN-CH-CN), 6.93 (d, J = 8.4 Hz, 4H, Ph-), 7.17 (d, J = 8.8 Hz, 4H, Ph-), 7.48 (t, J = 7.6 Hz, 2H, anthryl), 7.71 (t, J = 7.6 Hz, 2H, anthryl), 8.33 (br, 4H, anthryl). HRMS (ESI, m/z): [M - H]$^-$ calcd for $C_{39}H_{35}N_4$, 559.2862; found, 559.2861.

Fluorescence spectral measurements for the CN^- probing behavior

The fluorescence emission spectral changes of **C1~C5** during the titrations were measured at 25°C in the specified solutions, with the excitation wavelengths fixed at one of the corresponding isosbestic points. The slit width was 5 nm and PMT voltage was 600 V for both excitation and emission. Anions such as CN^-, F, Cl^-, Br^-, I^-, AcO^- and $H_2PO_4^-$ were added as TBA salts dissolved in the corresponding solvents. SCN^- and N_3^- were added as sodium salts. Fluorescence changes were measured after 30 min. To achieve the controlled pH for the aqueous solutions, three buffered systems were adopted in the measurements: tris-HCl, Na_2CO_3-$NaHCO_3$, and KCl-NaOH.

Detection Limits[7,8]

Detection limits of probes **C1~C3** were obtained according to the reported method. Taking **C3** as an example: **C3** (4 μM) was dissolved in a mixture of THF-H_2O (4:1 v/v). Fluorescence changes during the titration of **C3** (4 μM) with CN^- (0~32 μM) in THF-H_2O (4:1 v/v) are shown in Fig. S12e. Fluorescence enhancement is clearly resolved and there is a good signal-to-noise ratio. The inset of Figure S18a shows a plot of the fluorescence intensity versus [CN^-]. A linear regression curve was fitted to the seven intermediate values (4~18 μM CN^-) as shown in Fig. S12f. The standard deviation (σ = 0.2042) was obtained by fluorescence response (10-times of consecutive scanning on the Cary Eclipse fluorescence spectrophotometer). Thus, the detection limit of **C3** towards CN^- was calculated by the formula of 3σ/k to afford a value of 1.14 μM.

Determination of the fluorescence quantum yields[9]

Fluorescence quantum yield was determined using optically matched solutions of anthracene (Φ_r = 0.28 in ethanol), [10] Rhodamine 6G (Φ_r = 0.95 in ethanol), [11] and tetraphenylporphyrin (Φ_r = 0.11 in toluene), [12] as standards and the quantum yield was calculated using the following equation: $\Phi_s = \Phi_r(A_rF_s/A_sF_r)(n_s/n_r)^2$, where A_s and A_r are the absorbances of the samples and reference, respectively. At the excitation wavelength, F_s and F_r are the corresponding relative integrated fluorescence intensities, and n is the refractive index of the solvent.

DFT calculations

We employed density functional theory (DFT) calculations to study the cyanide probes. The hybrid B3LYP functional[13] was adopted to optimize molecular geometry in the ground state (S_0) and to calculate frontier molecular orbitals. The Ahlrichs split valence basis set[14] was used together with corresponding auxiliary basis sets,[15] and the "chain-of-spheres" algorithm[16] was used to speed up DFT calculations. Then time-dependent density functional theory (TDDFT) calculations were carried out to optimize the structures of these probes in the lowest singlet

excited state (S_1). All theoretical calculations were carried out using the ORCA program package.[17]

Kinetic measurements[18]

The reaction of the probe with CN^- was carried out at room temperature. The apparent rate constant for the reaction was determined by fitting the fluorescence of the samples to the pseudo first-order equation: $\ln[(F_{max}-F_0)/(F_{max}-F)] = kt$, where F_{max}, F_0 and F represent the fluorescence intensity at λ_{max} obtained after the reaction was complete, at time t, and before the addition of CN^-, respectively. k is the apparent rate constant. Taking **C3** as an example: time-dependent fluorescence changes were recorded and shown in Fig. S8a. And the plot of $\ln[(F_{max}-F_0)/(F_{max}-F)]$ *vs.* time t is shown Fig. S8b. Thus, the apparent rate constant k equals to the slope of 0.313 min^{-1}, which was obtained from the linear regression.

Crystallography

Single crystals of **C2** and **C3** suitable for X-ray analysis were obtained by slow evaporation of CH_3CN solution of **C2** or **C3** at room temperature.

CCDC-923724 (**C2**) and 923725 (**C3**) contain the supplementary crystallographic data for this paper. These data can be obtained free of charge from The Cambridge Crystallographic Data Centre via www.ccdc.cam.ac.uk/data_request/cif.

Crystal data for **C2**: $C_{27}H_{19}N_3O$, M_r = 401.45, Monoclinic, space group *P2(1)/c*, a = 14.1214(12), b = 10.6884(7), c = 14.2876(13) Å, β = 98.7490(10)°, V = 2131.4(3) $Å^3$, Z = 4, ρ_{calcd} = 1.251 g cm^{-3}, T = 298(2) K, 10480 measured reflections, 3748 unique reflections (R_{int}=0.0665); 1788 with I≥2σ(I) used in refinement, R_1 ($I > 2\sigma(I)$) = 0.0516, wR_2 (all data) = 0.1628, GOF = 1.048.

Crystal data for **C3**: $C_{40}H_{38}N_4$, M_r = 574.74, Monoclinic, space group *C2*, a = 25.741(2), b = 12.121(1), c = 11.444(1) Å, β = 96.976(1)°, V = 3544.4(6) $Å^3$, Z = 4, ρ_{calcd} = 1.077 g cm^{-3}, 9009 measured reflections, 3272 unique reflections (R_{int}=0.0649); 1715 with I≥2σ(I) used in refinement, R_1 ($I > 2\sigma(I)$) = 0.0688, wR_2 (all data) = 0.1910, GOF = 1.038.

References

1. S. Kolemen, Y. Cakmak, S. Erten-Ela, Y. Altay, J. Brendel, M. Thelakkat and E. U. Akkaya, *Org. Lett.,* 2010, **12**, 3812.
2. Y. J. Chang and T. J. Chow, *Tetrahedron,* 2009, **65**, 9626.
3. J. H. Lin, A. Elangovan and T. I. Ho, *J. Org. Chem.*, 2005, **70**, 7397.
4. H. C. Jeong, M. J. Piao, S. H. Lee, M. Y. Jeong, K. M. Kang, G. Park, S. J. Jeon and B. R. Cho, *Adv. Funct. Mater.,* 2004, **14**, 64.
5. J. Dauselt, J. L. Zhao, M. Kind, R. Binder, A. Bashir, A. Terfort and M. Zharnikov, *J. Phys. Chem. C,* 2011, **115**, 2841.
6. N. V. Tkachenko, H. Lemmetyinen, J. Sonoda, K. Ohkubo, T. Sato, H. Imahori and S. Fukuzumi, *J. Phys. Chem. A,* 2003, **107**, 8834.
7. C. Chen, R. Y. Wang, L. Q. Guo, N. Y. Fu, H. J. Dong and Y. F. Yuan, *Org. Lett.,* 2011, **13**, 1162.
8. J. Cao, C. C. Zhao, X. Z. Wang, Y. F. Zhang and W. H. Zhu, *Chem. Commun.,* 2012, **48**, 9897.
9. *(a)* J. N. Demas and G. A. Crosby, *J. Phys. Chem.,* 1971, **75**, 991; *(b)* D. F. Eaton, *Pure Appl.*

Chem., 1988, **60**, 1107.

10. C. A. Parker and W. T. Rees, *Analyst,* 1960, **85**, 587.
11. R. F. Kubin and A. N. Fletcher, *J. Lumin.*, 1982, **27**, 455.
12. *(a)* R. T. Kuznetsova, E. G. Ermolina, R. M. Gadirov, G. V. Mayer, N. N. Semenishin, S. A. Zhuravlev, N. V. Rusakova and Y. V. Korovin, *Optics and Spectroscopy,* 2009, **106**, 672; *(b)* R. R. Valiev, V. N. Cherepanov, V. Y. Artyukhov and D. Sundholm, *Phys. Chem. Chem. Phys.,* 2012, **14**, 11508.
13. A. D. Becke, *J. Chem. Phys.,* 1993, **98**, 5648.
14. A. Schäfer, H. Horn and R. Ahlrichs, *J. Chem. Phys.,* 1992, **97**, 2571.
15. *(a)* K. Eichkorn, O. Treutler, H. Ohm, M. Haser and R. Ahlrichs, *Chem. Phys. Lett.,* 1995, **240**, 283; *(b)* K. Eichkorn, F. Weigend, O. Treutler and R. Ahlrichs, *Theor. Chem. Acc.,* 1997, **97**, 119.
16. F. Neese, F. Wennmohs, A. Hansen and U. Becker, *Chem. Phys.,* 2009, **356**, 98.
17. ORCA, An *ab initio*, DFT and semiempirical SCF-MO package, version 2.9, http://www.thch.uni-bonn.de/tc/orca/.
18. *(a)* Z. P. Liu, X. Q. Wang, Z. H. Yang, and W. J. He, *J. Org. Chem.*, 2011, **76**, 10286; *(b)* M. Dong, Y. Peng, Y. M. Dong, N. Tang, and Y. W. Wang, *Org. Lett.*, 2012, **14**, 130.

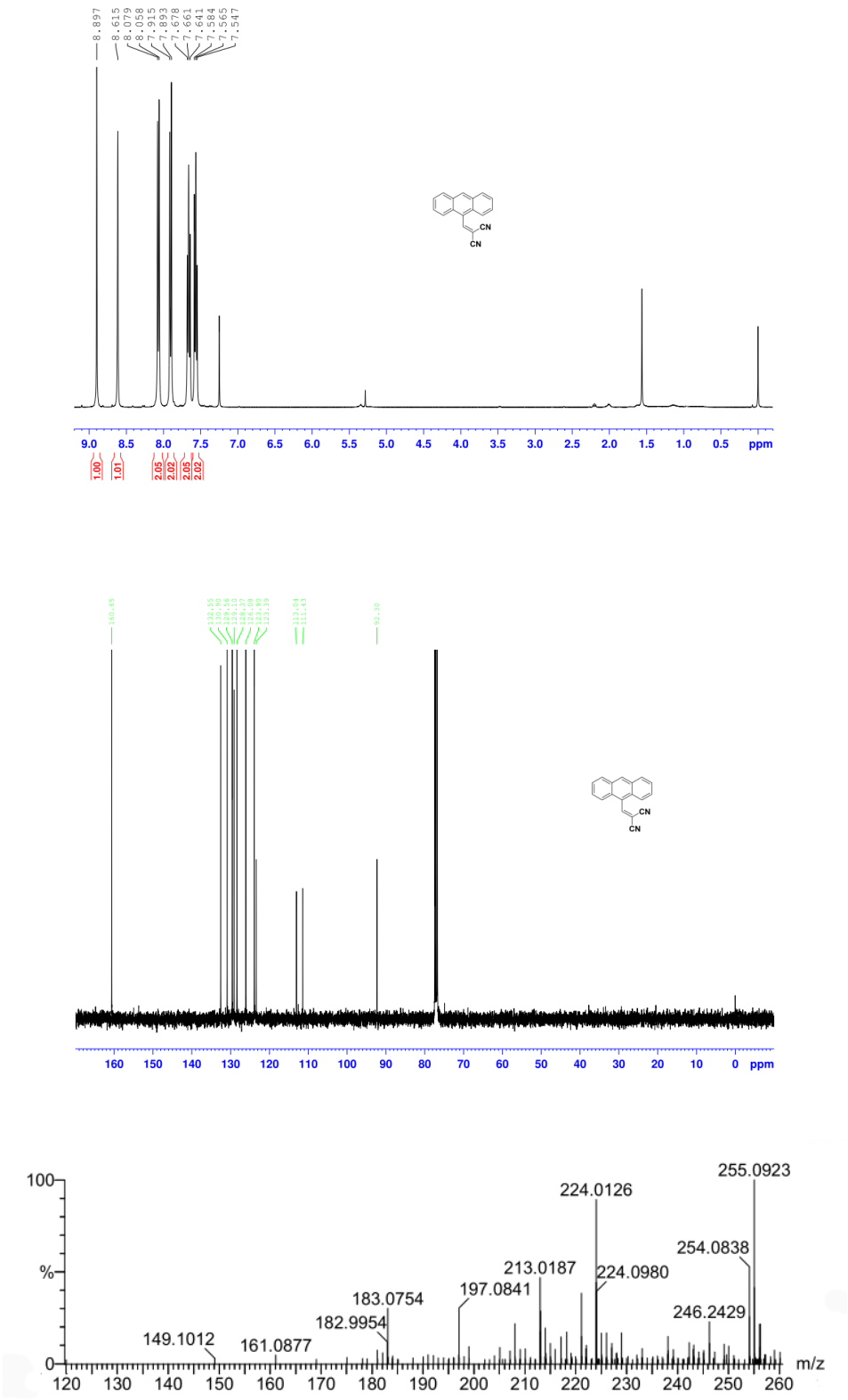

Fig. S1. Characterization data for **C1**

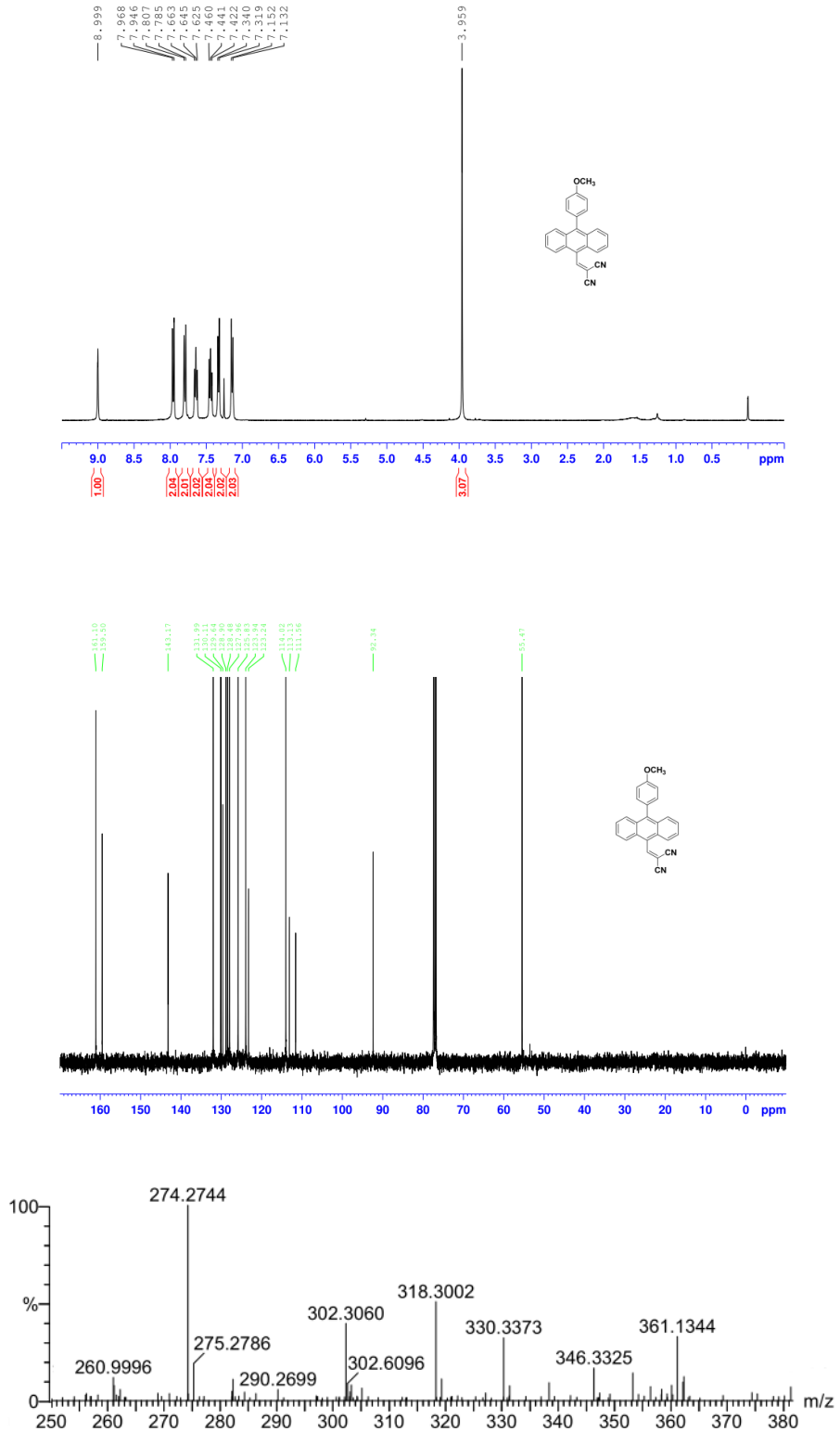

Fig. S2. Characterization data for **C2**

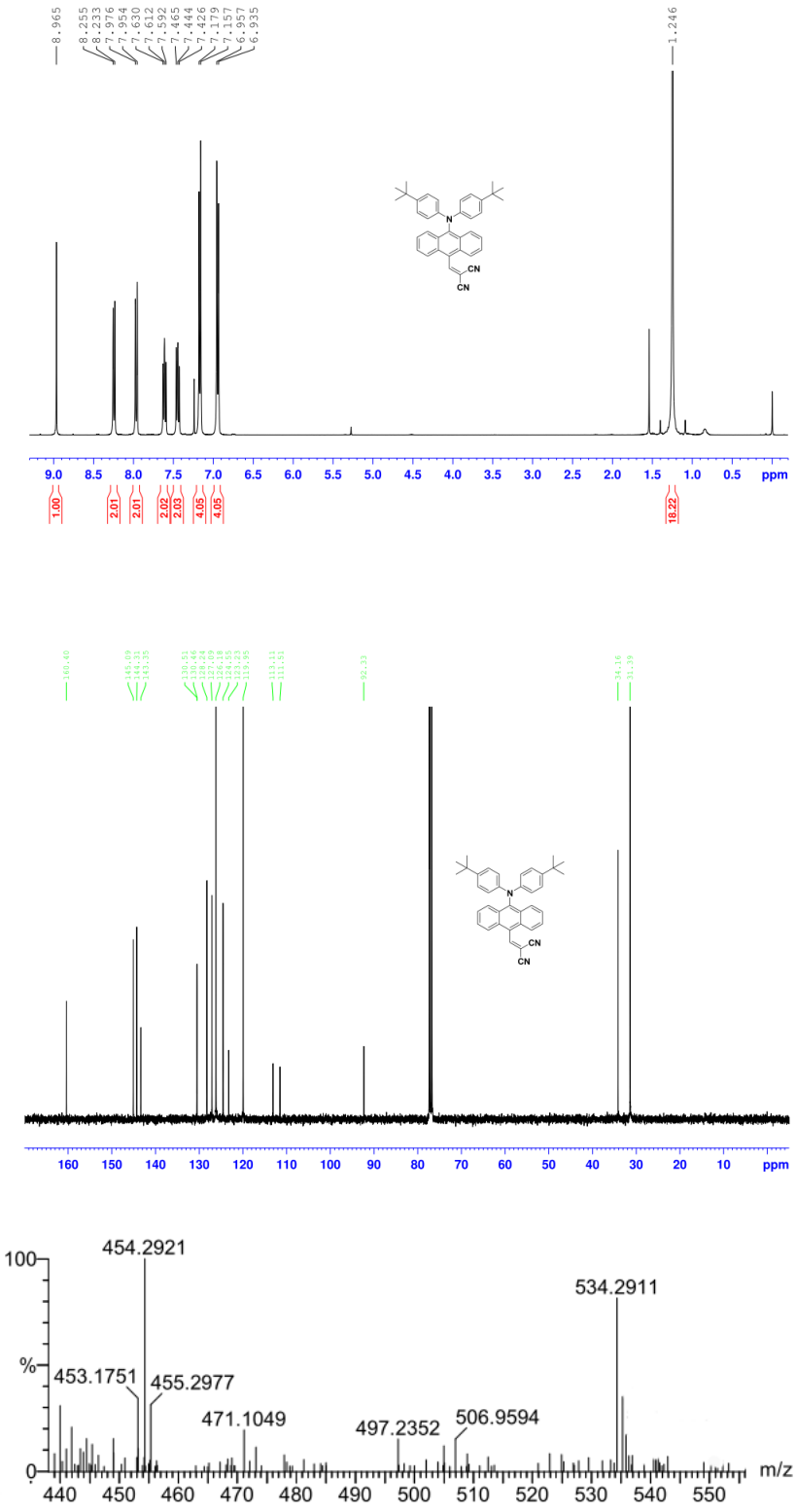

Fig. S3. Characterization data for **C3**

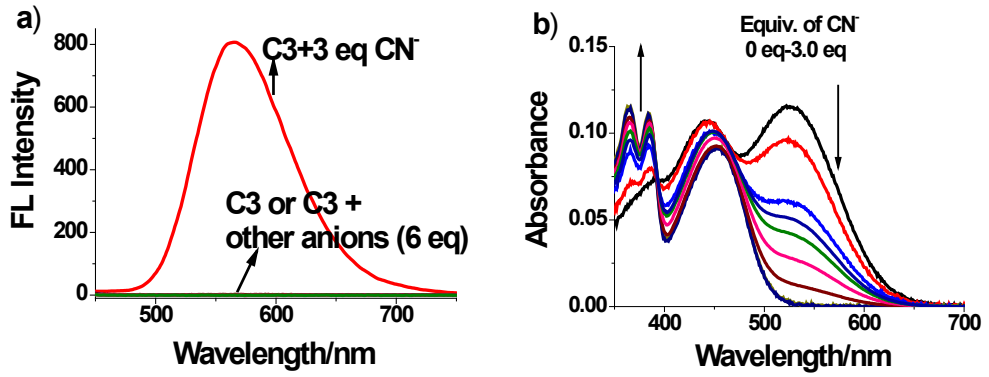

Fig. S4. a) Fluorescence of **C3** (20 μM) in CH_2Cl_2 in the presence of anions (6 eq. each, except 3 eq. of CN^-). λ_{ex} = 396 nm. b) Absorption spectral changes during the titration of **C3** (20 μM) with CN^- in CH_2Cl_2.

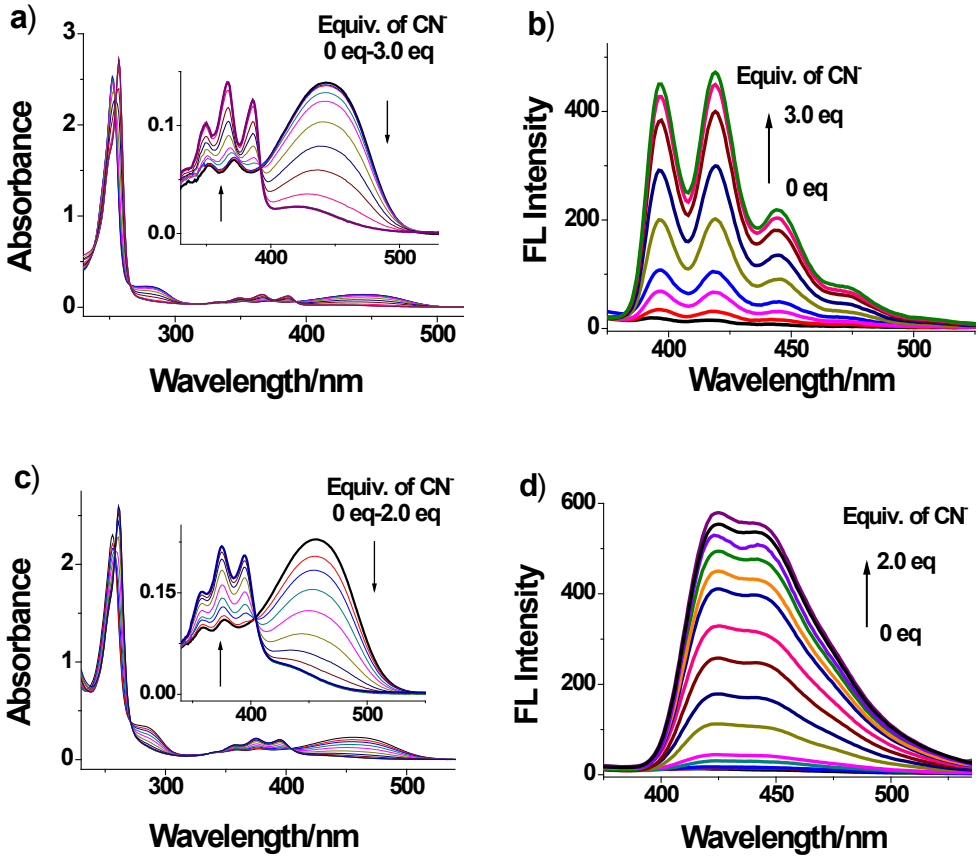

Fig. S5. a) Absorption spectral changes during the titration of **C1** (20 μM) with CN^- in CH_2Cl_2. Inset: part of absorption spectral changes. b) Fluorescence changes during the titration of **C1** (20 μM) with CN^- in CH_2Cl_2. Excitation wavelength was fixed at 266 nm (one of the isosbestic points) during titration. c) Absorption spectral changes during the titration of **C2** (20 μM) with CN^- in CH_2Cl_2. Inset: part of absorption spectral changes. d) Fluorescence changes during the titration of **C2** (20 μM) with CN^- in CH_2Cl_2. Excitation wavelength was fixed at 272 nm (one of the isosbestic points) during titration.

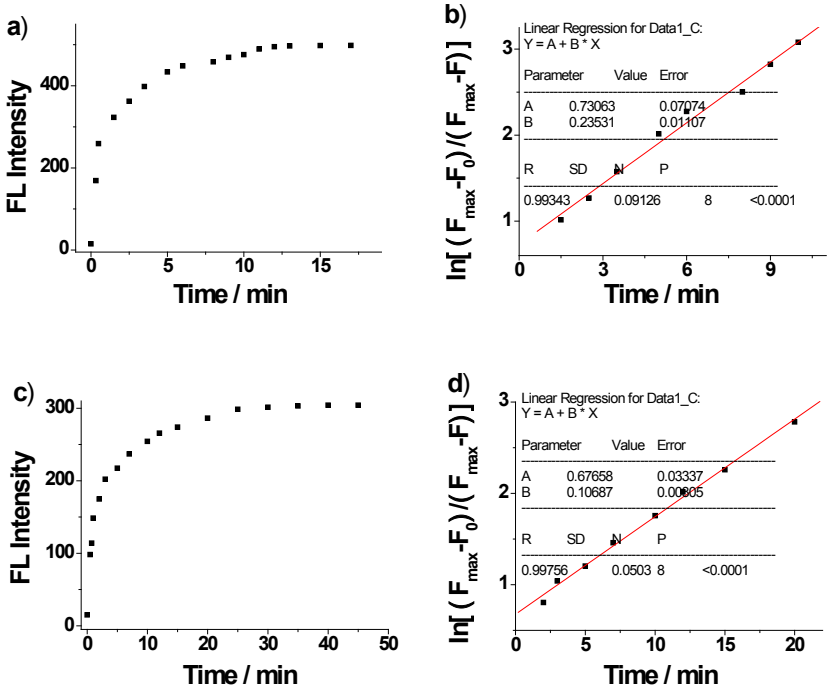

Fig. S6. Time course of the fluorescence response of **C1** (20 μM) in CH_2Cl_2 upon addition of (a) 3 equiv. or (c) 1.5 equiv. of CN^- (λ_{ex} = 266 nm, λ_{em} = 419 nm) with the corresponding kinetic analysis according to the pseudo-first-order model. ((b) k = 0.235 min^{-1} obtained from (a), and (d) k = 0.107 min^{-1} obtained from (c)).

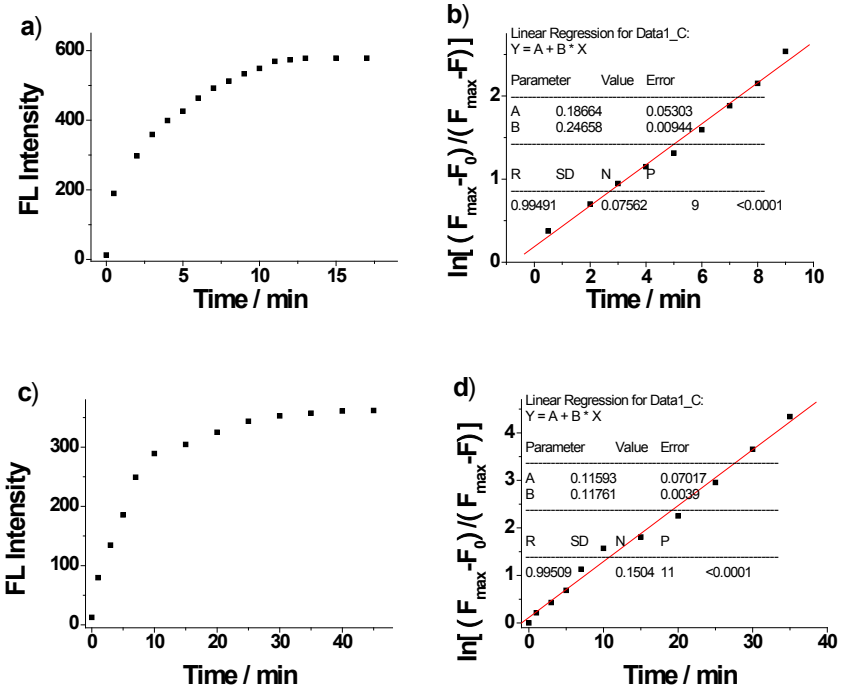

Fig. S7. Time course of the fluorescence response of **C2** (20 μM) in CH_2Cl_2 upon addition of (a) 2 equiv. or (c) 1 equiv. of CN^- (λ_{ex} = 272 nm, λ_{em} = 423 nm) with the corresponding kinetic analysis according to the pseudo-first-order model. ((b) k = 0.191 min^{-1} obtained from (a), and (d) k = 0.118 min^{-1} obtained from (c))

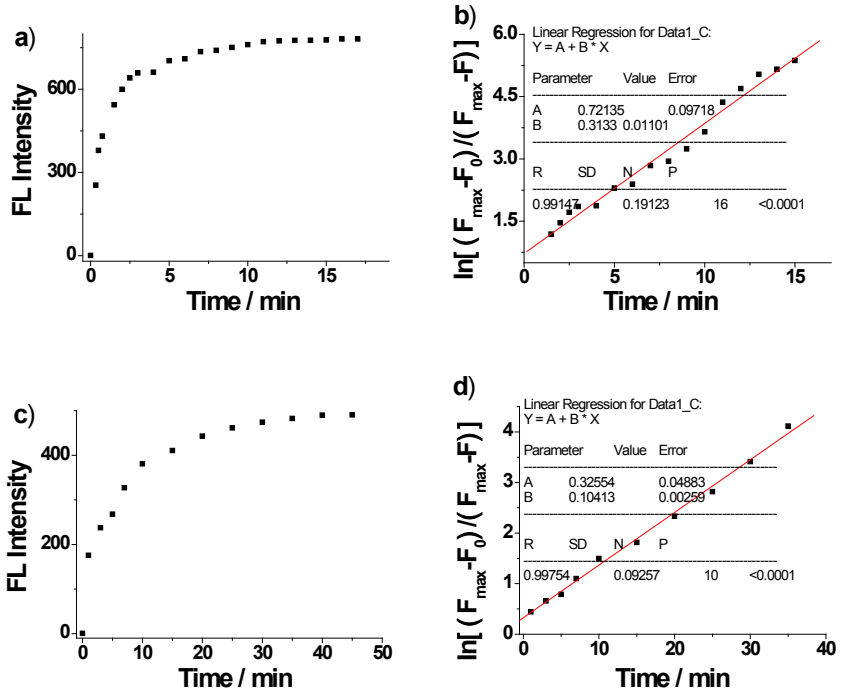

Fig. S8. Time course of the fluorescence response of **C3** (20 μM) in CH_2Cl_2 upon addition of (a) 3 equiv. or (c) 1.5 equiv. of CN^- (λ_{ex} = 396 nm, λ_{em} = 564 nm) with the corresponding kinetic analysis according to the pseudo-first-order model. ((b) k = 0.313 min^{-1} obtained from (a), and (d) k = 0.104 min^{-1} obtained from (c)).

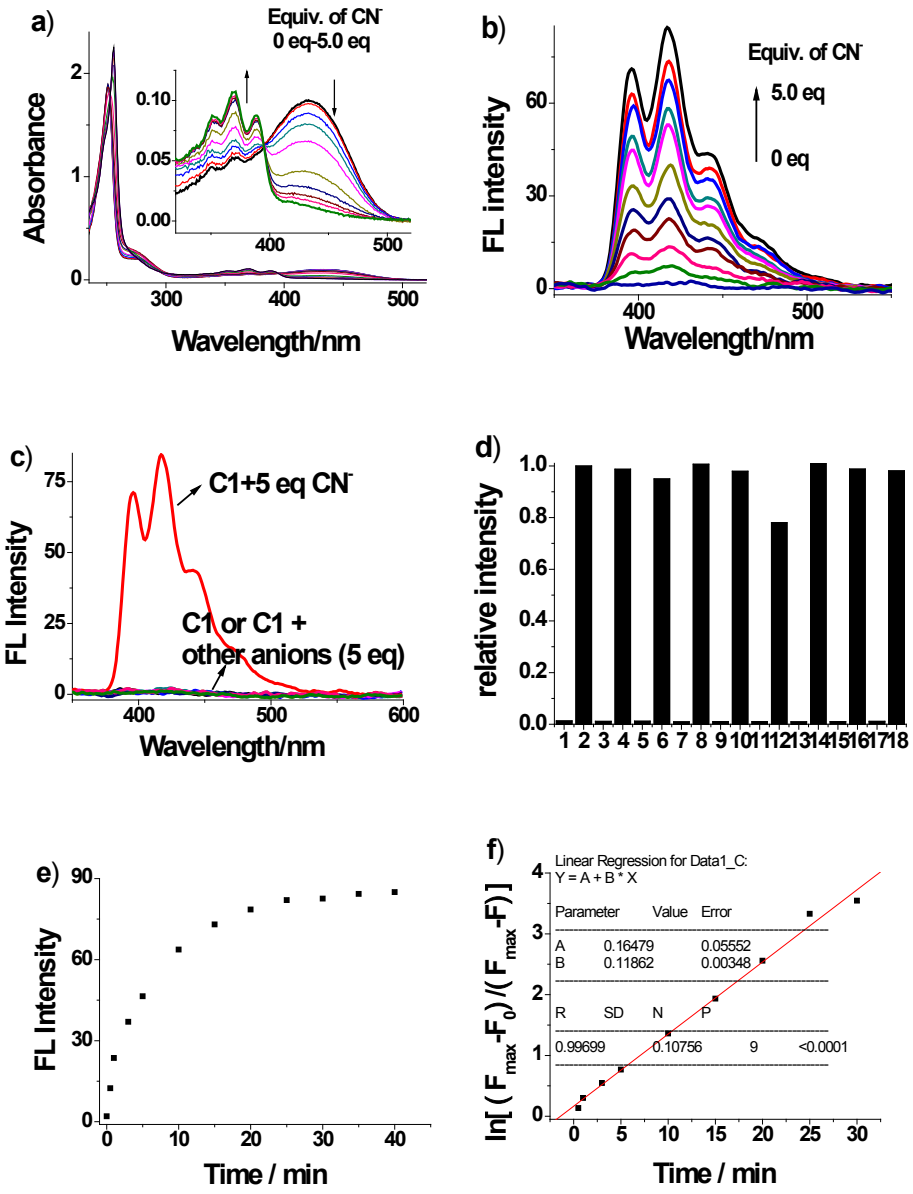

Fig. S9. a) Absorption spectral changes during the titration of **C1** (20 μM) with CN^- in THF-H_2O (4:1 v/v). Inset: partial absorption spectral changes. b) Fluorescence changes during the titration of **C1** (20 μM) with CN^- in THF-H_2O (4:1 v/v). c) Fluorescence spectra of **C1** (20 μM) in the presence of various anions in THF-H_2O (4:1 v/v). d) Relative fluorescence intensity of **C1** (20 μM) in THF-H_2O (4:1 v/v): odd numbers represent none or 5 equiv anions, even number represent 5 equiv CN^- or 5 equiv CN^- with 5 equiv other anions (F^-, Cl^-, Br^-, I^-, CH_3COO^-, $H_2PO_4^-$, N_3^-, SCN^-). Excitation wavelength was fixed at 253 nm (one of the isosbestic points) during the fluorescence measurements. e) Time course of the fluorescence response of **C1** (20 μM) in THF-H_2O (4:1 v/v) upon addition of 5 equiv. of CN^- (λ_{ex} = 253 nm, λ_{em} = 417 nm). f) The kinetic analysis according to the pseudo-first-order model (k = 0.119 min^{-1}).

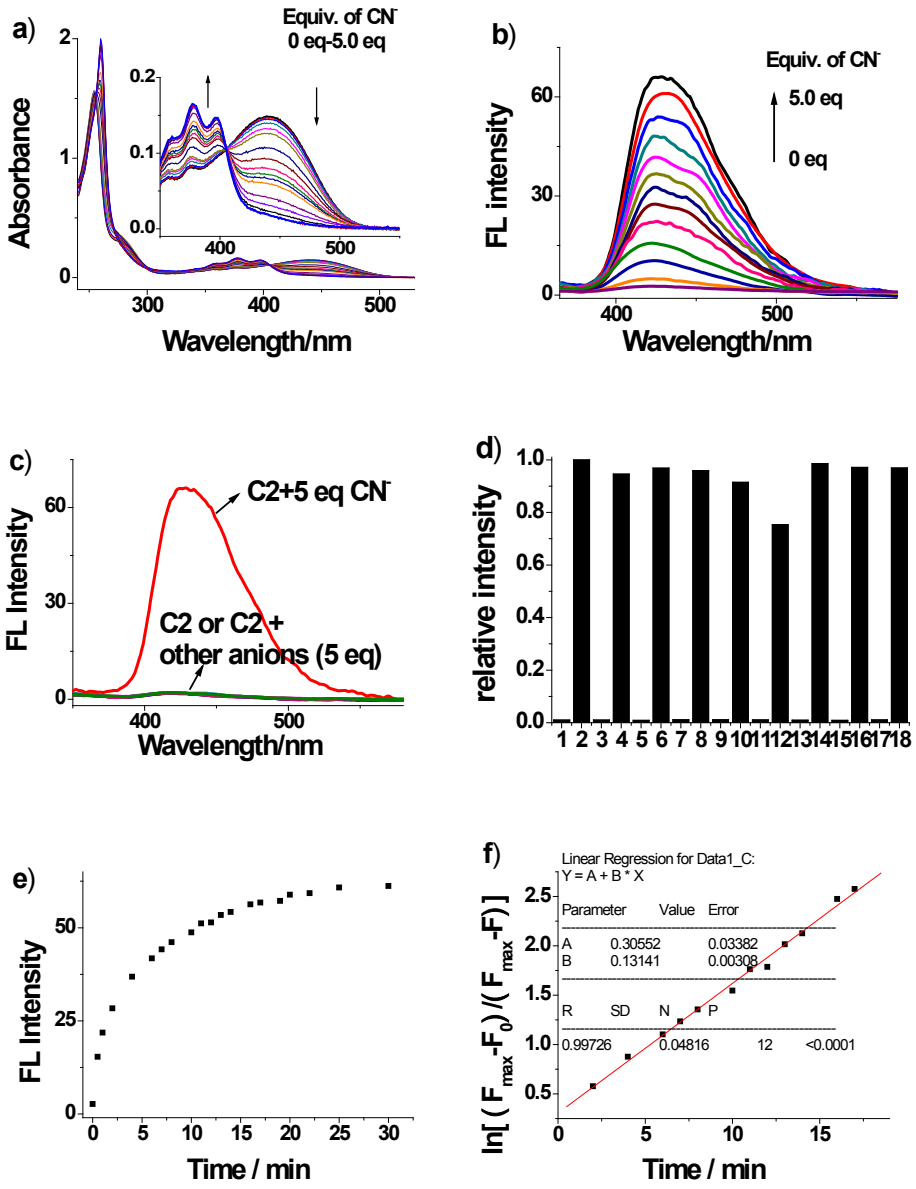

Fig. S10. a) Absorption spectral changes during the titration of **C2** (20 μM) with CN^- in THF-H_2O (4:1 v/v). Inset: partial absorption spectral changes. b) Fluorescence changes during the titration of **C2** (20 μM) with CN^- in THF-H_2O (4:1 v/v). c) Fluorescence spectra of **C2** (20 μM) in the presence of various anions in THF-H_2O (4:1 v/v). d) Relative fluorescence intensity of **C2** (20 μM) in THF-H_2O (4:1 v/v): odd numbers represent none or 5 equiv anions, even number represent 5 equiv CN^- or 5 equiv CN^- with 5 equiv other anions (F^-, Cl^-, Br^-, I^-, CH_3COO^-, $H_2PO_4^-$, N_3^-, SCN^-). Excitation wavelength was fixed at 256 nm (one of the isosbestic points) during the fluorescence measurements. e) Time course of the fluorescence response of **C2** (20 μM) in THF-H_2O (4:1 v/v) upon addition of 5 equiv. of CN^- (λ_{ex} = 256 nm, λ_{em} = 425 nm). f) The kinetic analysis according to the pseudo-first-order model (k = 0.131 min^{-1}).

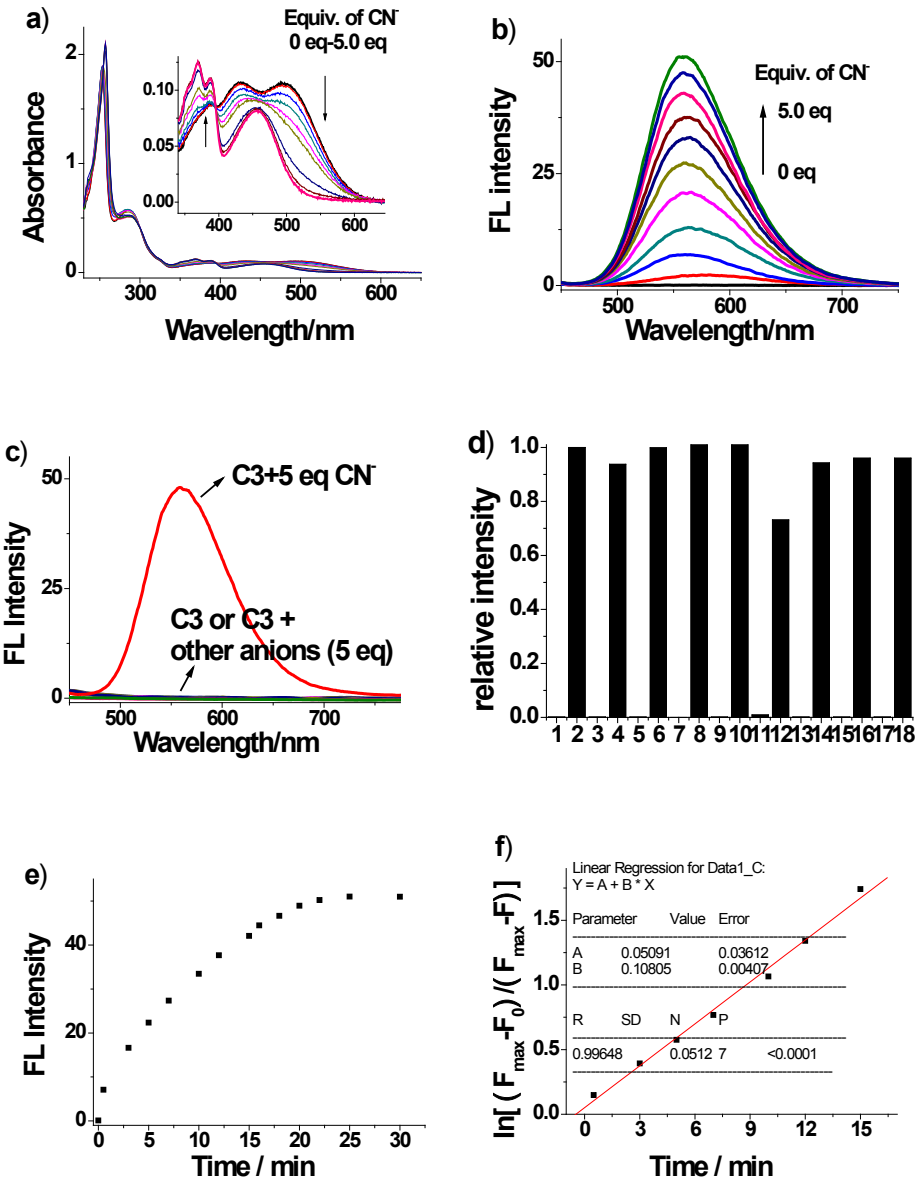

Fig. S11. a) Absorption spectral changes during the titration of **C3** (20 μM) with CN^- in THF-H_2O (4:1 v/v). Inset: partial absorption spectral changes. b) Fluorescence changes during the titration of **C3** (20 μM) with CN^- in THF-H_2O (4:1 v/v). c) Fluorescence spectra of **C3** (20 μM) in the presence of various anions in THF-H_2O (4:1 v/v). d) Relative fluorescence intensity of **C3** (20 μM) in THF-H_2O (4:1 v/v): odd numbers represent none or 5 equiv anions, even number represent 5 equiv CN^- or 5 equiv CN^- with 5 equiv other anions (F^-, Cl^-, Br^-, I^-, CH_3COO^-, $H_2PO_4^-$, N_3^-, SCN^-). Excitation wavelength was fixed at 396 nm (one of the isosbestic points) during the fluorescence measurements. e) Time course of the fluorescence response of **C3** (20 μM) in THF-H_2O (4:1 v/v) upon addition of 5 equiv. of CN^- (λ_{ex} = 396 nm, λ_{em} = 560 nm). f) The kinetic analysis according to the pseudo-first-order model (k = 0.108 min^{-1}).

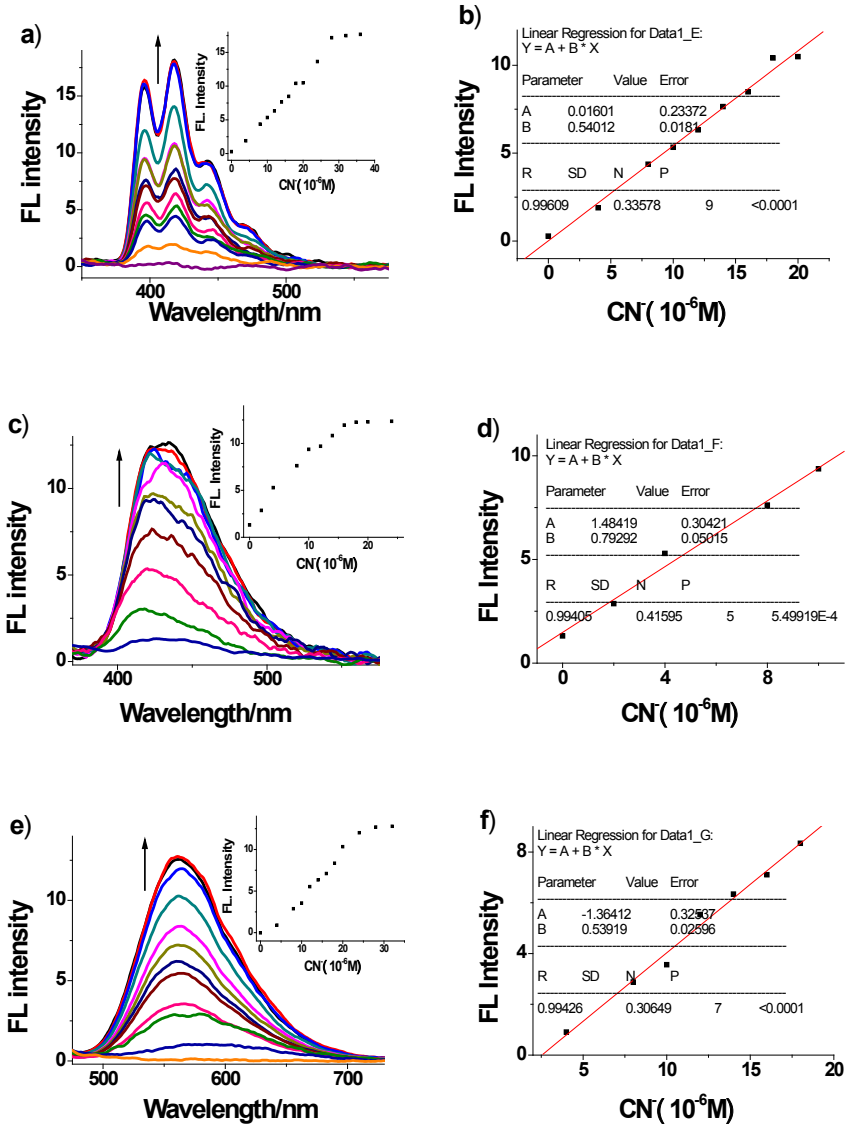

Fig. S12. a) Fluorescence changes during the titration of **C1** (4 μM) with CN^- (0~36 μM) in THF-H_2O (4:1 v/v), inset: fluorescence intensity between the minimum (free **C1**) and the maximum values (24 μM CN^- added). b) A plot of I vs [CN^-], the calculated detection limit of probe **C1** is 2.46 μM (σ = 0.4431). c) Fluorescence changes during the titration of **C2** (4 μM) with CN^- (0~24 μM) in THF-H_2O (4:1 v/v), inset: fluorescence intensity between the minimum (free **C2**) and the maximum values (24 μM CN^- added). d) A plot of I vs [CN^-], the calculated detection limit of probe **C2** is 1.29 μM (σ = 0.3401). e) Fluorescence changes during the titration of **C3** (4 μM) with CN^- (0~32 μM) in THF-H_2O (4:1 v/v), inset: fluorescence intensity between the minimum (free **C3**) and the maximum values (32 μM CN^- added). f) A plot of I vs [CN^-], the calculated detection limit of probe **C3** is 1.14 μM (σ = 0.2042).

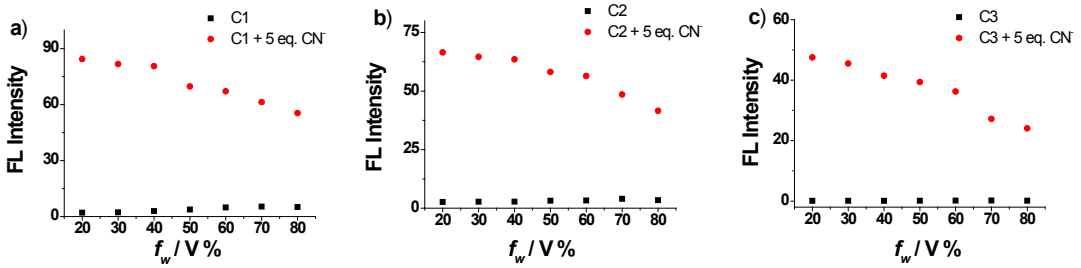

Fig. S13. Plots of the fluorescence intensities of the probes *vs.* the water content f_w in the THF-water mixtures. a) **C1** (20 μM, black squares), **C1**+5 eq CN^- (red circles) (λ_{ex} = 253 nm, λ_{em} = 417 nm). b) **C2** (20 μM, black squares), **C2**+5 eq CN^- (red circles) (λ_{ex} = 256 nm, λ_{em} = 425 nm). c) **C3** (20 μM, black squares), **C3**+5 eq CN^- (red circles) (λ_{ex} = 396 nm, λ_{em} = 560 nm).

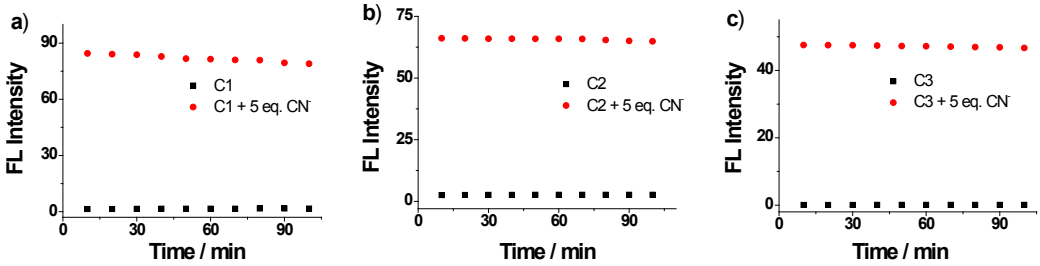

Fig. S14. Time-dependent fluorescence intensities of the probes in THF-H_2O (4:1 v/v) under the 365 nm UV irradiation. a) **C1** (20 μM, black squares), **C1**+5 eq CN^- (red circles) (λ_{ex} = 253 nm, λ_{em} = 417 nm) b) **C2** (20 μM, black squares), **C2**+5 eq CN^- (red circles) (λ_{ex} = 256 nm, λ_{em} = 425 nm). c) **C3** (20 μM, black squares), **C3**+5 eq CN^- (red circles) (λ_{ex} = 396 nm, λ_{em} = 560 nm).

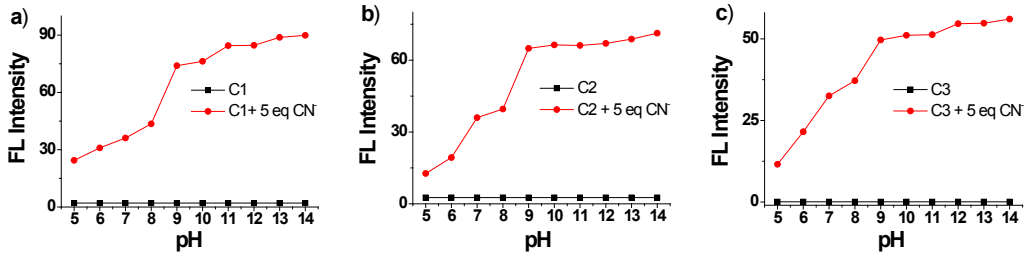

Fig. S15. The fluorescence intensities of probes over the pH range of 5-14 in THF-H_2O (4:1 v/v). a) **C1** (20 μM, black squares), **C1**+5 eq CN^- (red circles) b) **C2** (20 μM, black squares), **C2**+5 eq CN^- (red circles) c) **C3** (20 μM, black squares), **C3**+5 eq CN^- (red circles).

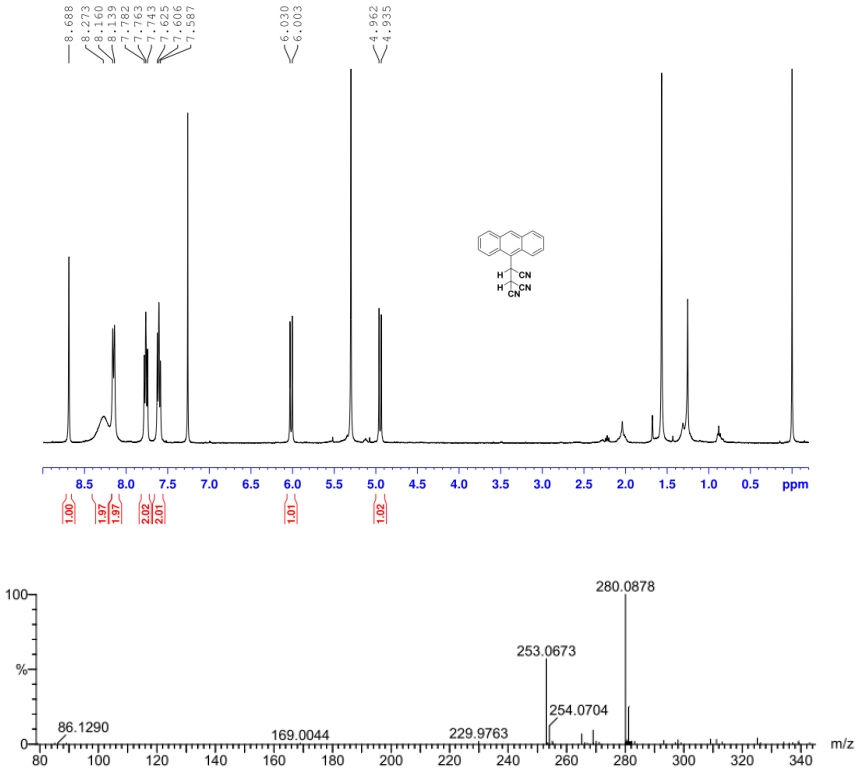

Fig. S16. Characterization data for **C1-CN**

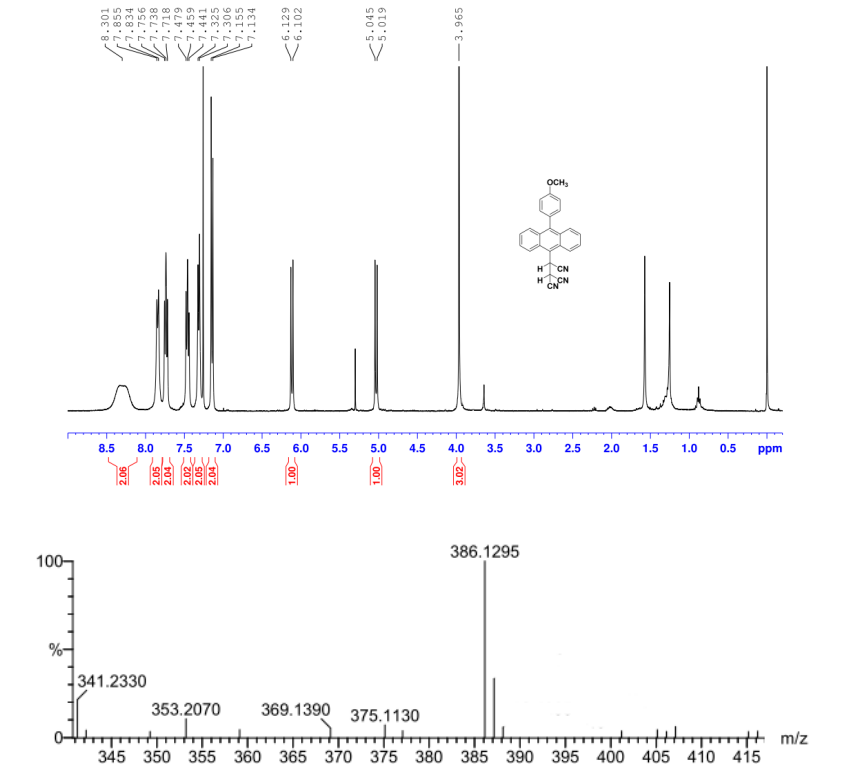

Fig. S17. Characterization data for **C2-CN**

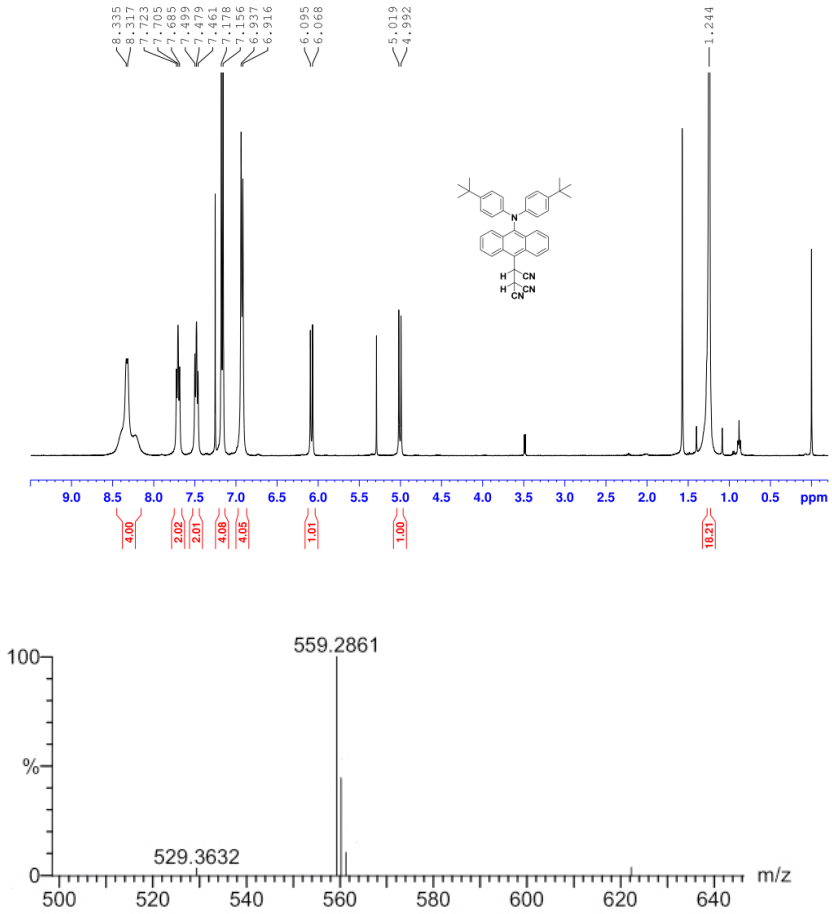

Fig. S18. Characterization data for **C3-CN**

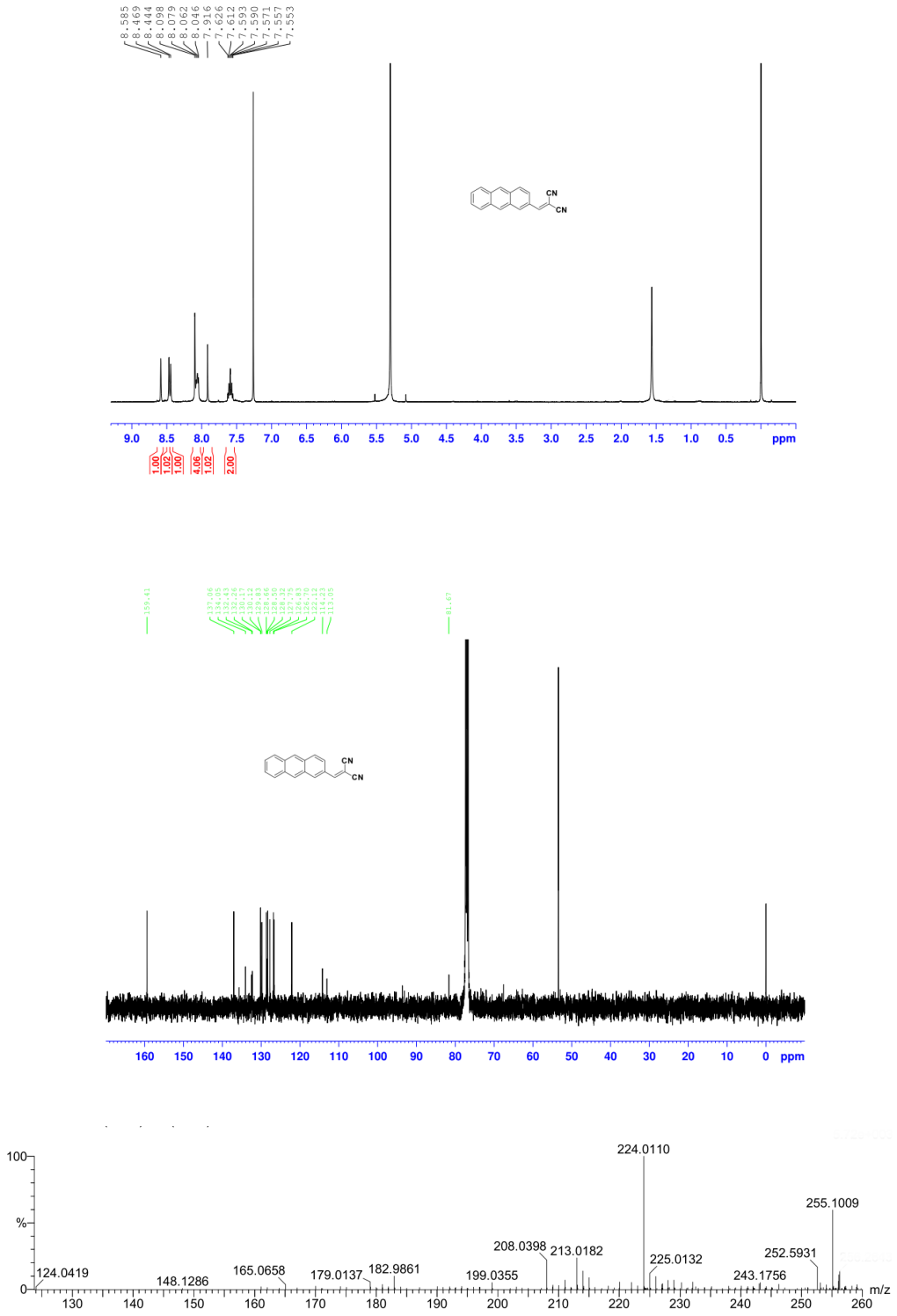

Fig. S19. Characterization data for **C4**

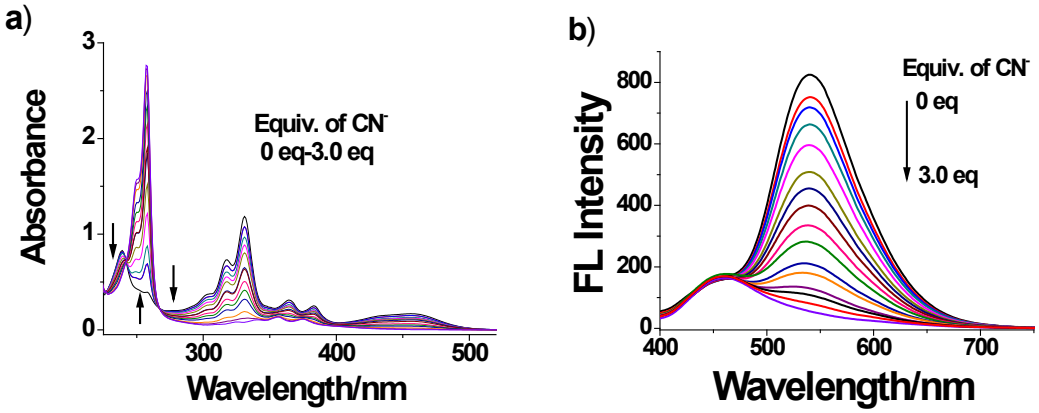

Fig. S20. a) Absorption spectral changes during the titration of **C4** (20 μM) with CN^- in CH_2Cl_2. b) Fluorescence changes during the titration of **C4** (20 μM) with CN^- in CH_2Cl_2. Excitation wavelength was fixed at 272 nm during titration.

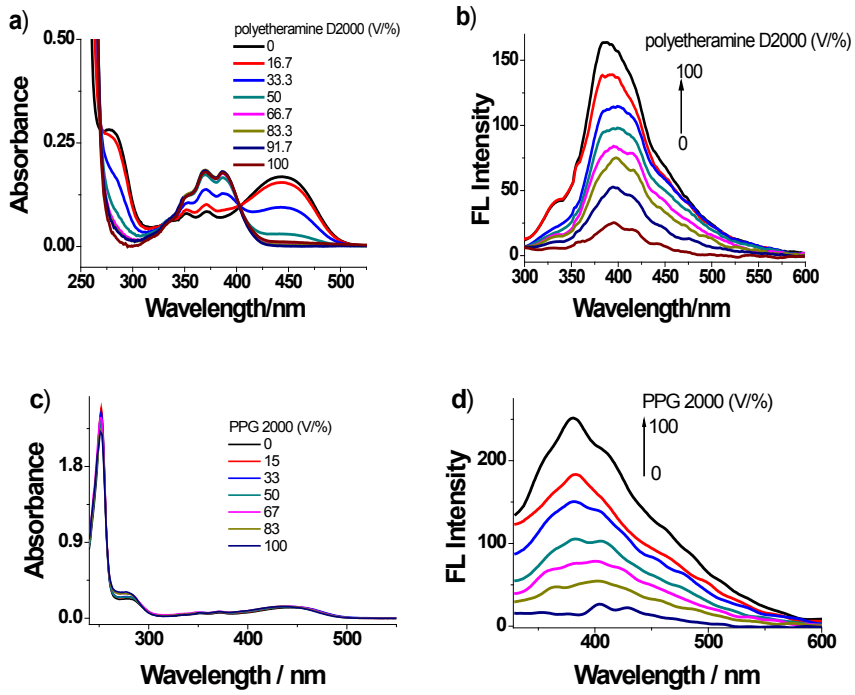

Fig. S21. a) Absorption spectral changes of **C1** (20 μM) in dichloromethane/polyetheramine D2000 with increasing viscosity. b) Fluorescence of **C1** (20 μM) in dichloromethane/polyetheramine D2000 with increasing viscosity (λ_{ex} = 269 nm). c) Absorption spectral changes of **C1** (20 μM) in dichloromethane/polypropylene glycol 2000 with increasing viscosity. Inset: absorption spectra of **C1** in CH_2Cl_2 or PPG 2000. d) Fluorescence of **C1** (20 μM) in dichloromethane/ polypropylene glycol 2000 with increasing viscosity (λ_{ex} = 323 nm).

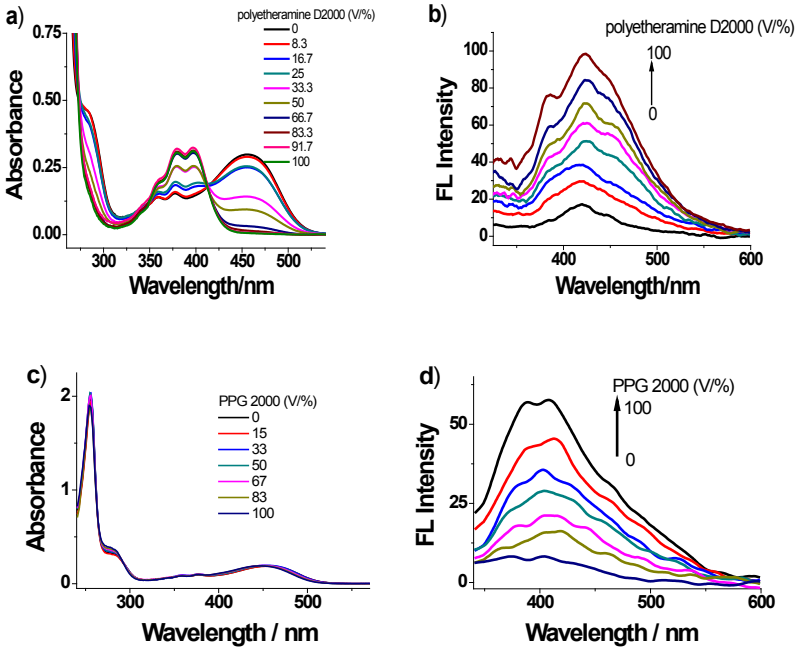

Fig. S22. a) Absorption spectral changes of **C2** (20 μM) in dichloromethane/polyetheramine D2000 with increasing viscosity. b) Fluorescence of **C2** (20 μM) in dichloromethane/polyetheramine D2000 with increasing viscosity (λ_{ex} = 274 nm). c) Absorption spectral changes of **C2** (20 μM) in dichloromethane/polypropylene glycol 2000 with increasing viscosity. Inset: absorption spectra of **C2** in CH_2Cl_2 or PPG 2000. d) Fluorescence of **C2** (20 μM) in dichloromethane/ polypropylene glycol 2000 with increasing viscosity (λ_{ex} = 330 nm).

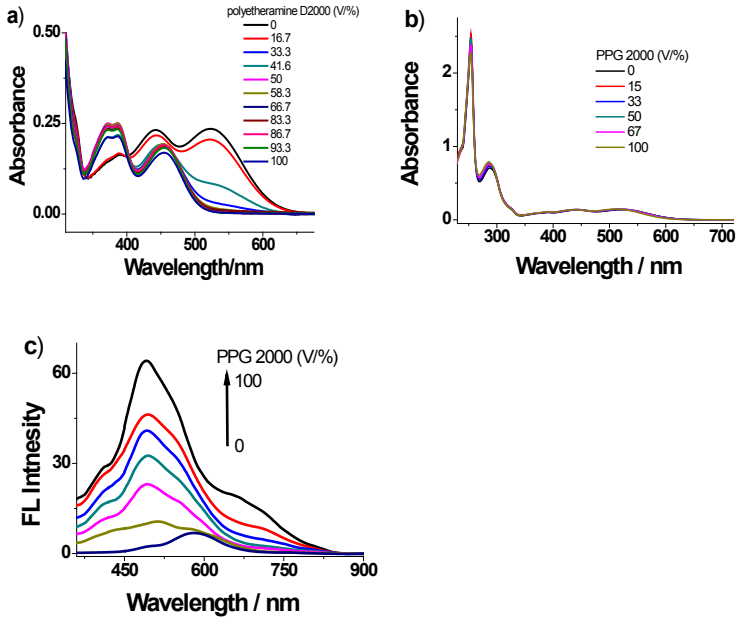

Fig. S23. a) Absorption spectral changes of **C3** (20 μM) in dichloromethane/polyetheramine D2000 with increasing viscosity. b) Absorption spectral changes of **C3** (20 μM) in dichloromethane/polypropylene glycol 2000 with increasing viscosity. Inset: absorption spectra of **C3** in CH_2Cl_2 or PPG 2000. c) Fluorescence of **C3** (20 μM) in dichloromethane/ polypropylene glycol 2000 with increasing viscosity (λ_{ex} = 350 nm).

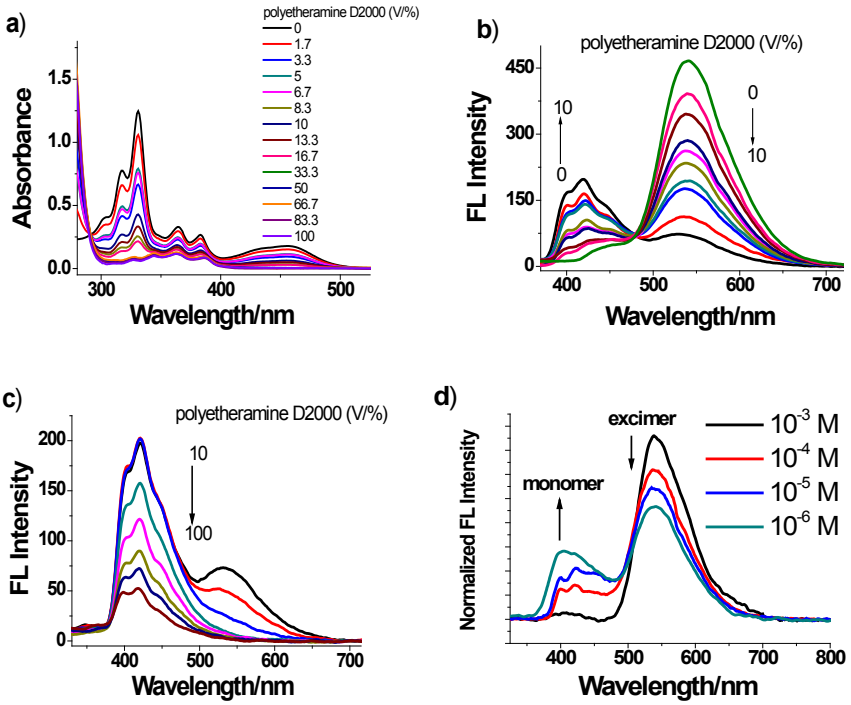

Fig. S24. a) Absorption spectral changes of **C4** (20 μM) in dichloromethane/polyetheramine D2000 with increasing viscosity. b) Fluorescence spectral changes with varying viscosity in a mixture of dichloromethane/ polyetheramine D2000 for a) **C3** (20 μM, λ_{ex} = 401 nm); b) **C4** (20 μM, λ_{ex} = 291 nm).c) Fluorescence of **C4** (20 μM) in dichloromethane/polyetheramine D2000 (10~100%) with increasing viscosity (λ_{ex} = 291 nm). d) Normalized emission of **C4** in dichloromethane showing the increasing ratio of monomer:excimer with decreasing concentration (λ_{ex} = 272 nm).

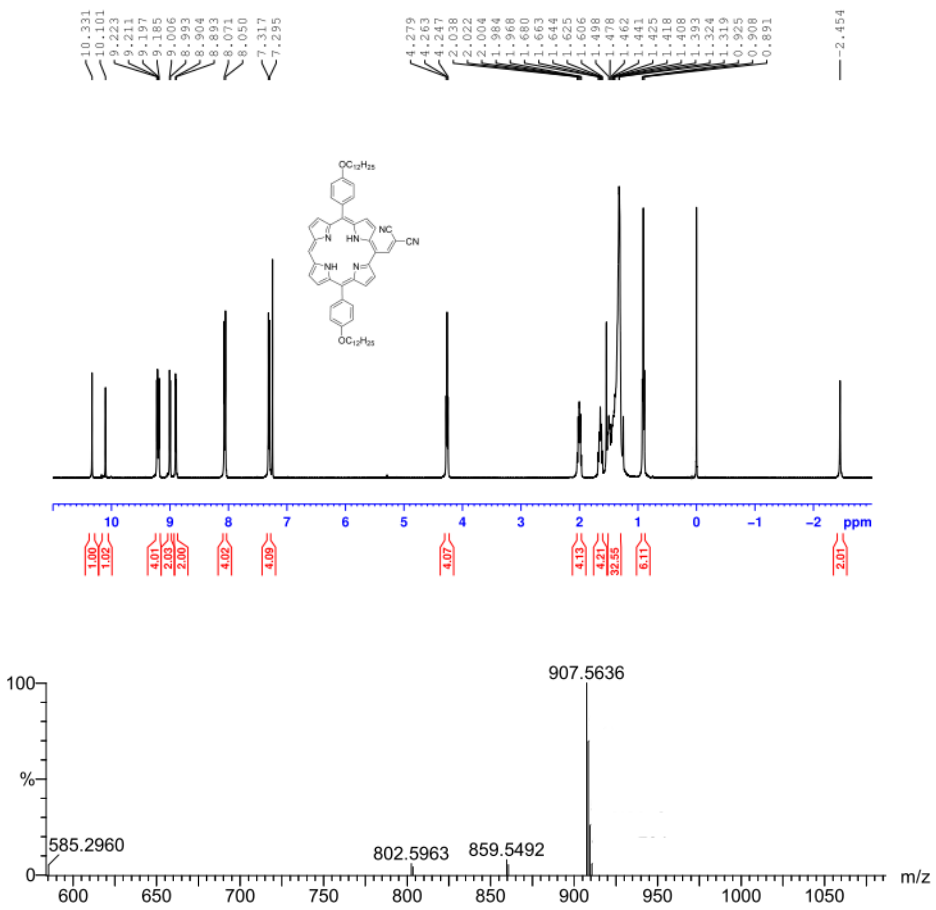

Fig. S25. Characterization data for **C5**

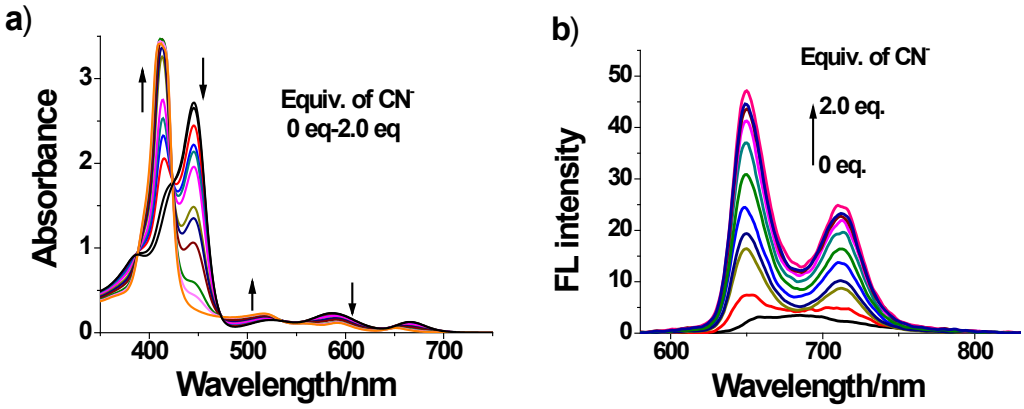

Fig. S26. a) Absorption spectral changes during the titration of **C5** (20 μM) with CN^- in CH_2Cl_2. b) Fluorescence changes during the titration of **C5** (20 μM) with CN^- in CH_2Cl_2. Excitation wavelength was fixed at 423 nm during titration.

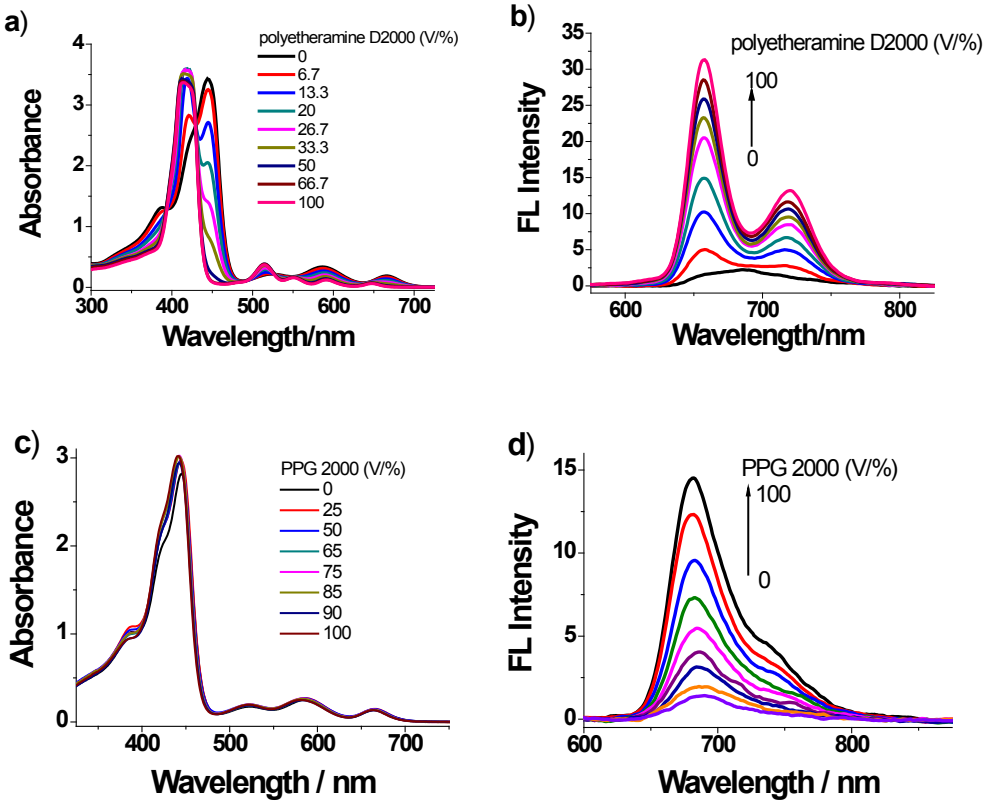

Fig. S27. a) Absorption spectral changes of **C5** (20 μM) in dichloromethane/polyetheramine D2000 with increasing viscosity. b) Fluorescence of **C5** (20 μM) in dichloromethane/polyetheramine D2000 with increasing viscosity with (λ_{ex} = 527 nm). c) Absorption spectral changes of **C5** (20 μM) in dichloromethane/polypropylene glycol 2000 with increasing viscosity. Inset: absorption spectra of **C5** in CH_2Cl_2 or PPG 2000. d) Fluorescence of **C5** (20 μM) in dichloromethane/ polypropylene glycol 2000 with increasing viscosity (λ_{ex} = 447 nm).

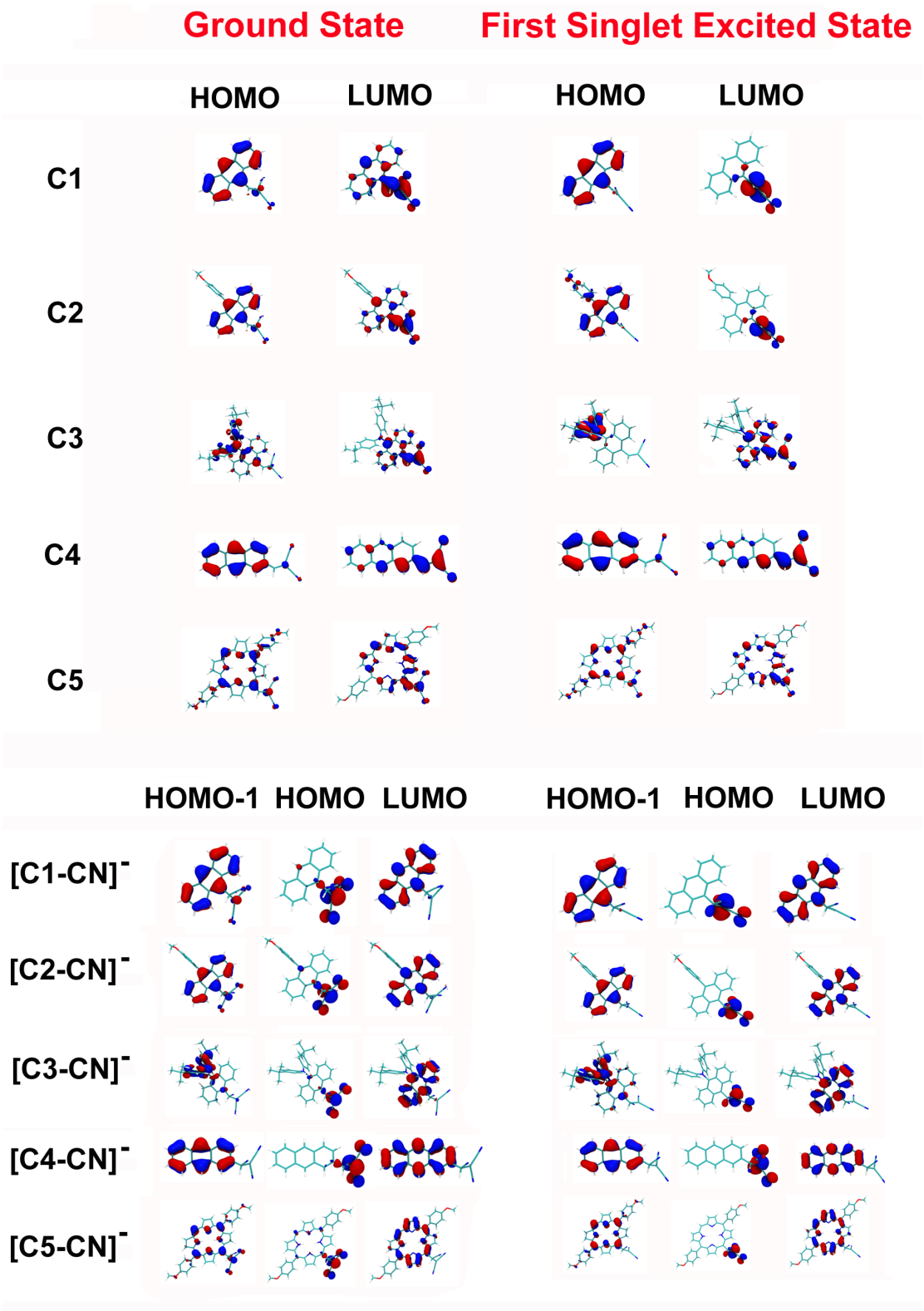

Fig. S28. Frontier molecular orbitals of compounds **C1~C5** and [**C1-CN**]$^-$~[**C5-CN**]$^-$.

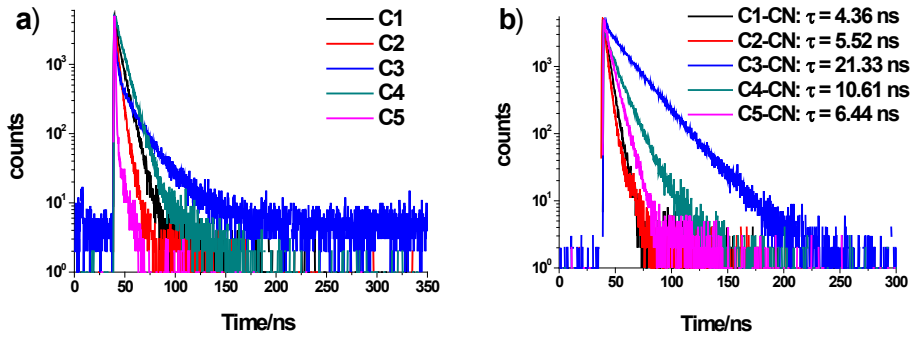

Fig. S29. Fluorescence decay curves for a) probes **C1~C5** (10 μM) in dichloromethane; b) probes **C1~C5** (10 μM) after addition of 3 eq. CN^- in dichloromethane.

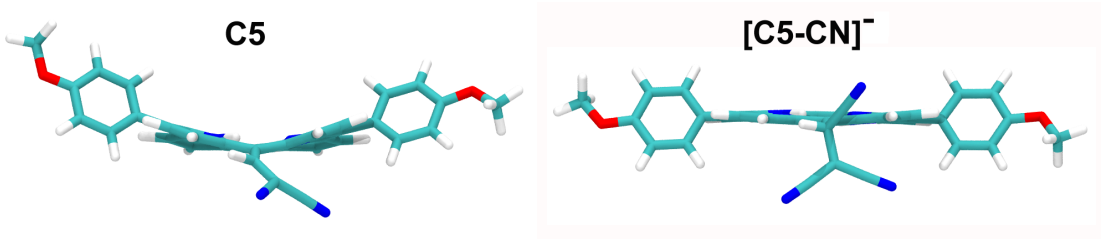

Fig. S30. Optimized structures of compounds **C5** (left) and **[C5-CN]**$^-$ (right).

Table S1. Quantum yields of probes **C1~C3** and their CN^- adducts formed upon addition of 3 eq. CN^- in various solvents.

entry	Φ_F/% CH_2Cl_2	Φ_F/% THF	Φ_F/% CH_3OH	Φ_F/% DMF	Φ_F/% ACN
C1	0.49	0.47	0.45	0.44	0.32
C1-CN	11.4	9.8	4.1	3.7	2.8
C2	0.42	0.40	0.40	0.36	0.32
C2-CN	20.1	18.7	7.0	6.9	6.7
C3	0.065	0.06	0.05	0.04	0.034
C3-CN	14.1	7.2	4.0	3.5	3.4

Table S2. Dihedral angles in the optimized ground state (S_0) and the lowest singlet excited state (S_1) structures, optimized at the B3LYP/SV(P) and TD-B3LYP/SV(P) level, respectively.(φ denotes the dihedral angle between the anthryl and the DCV units, ψ denotes the dihedral angle between the anthryl unit and the donor or that between the porphyrin and the phenyl unit.)

Compound	φ		ψ[a]	
	S_0	S_1	S_0	S_1
C1	53.8°	88.1°	/	/
C2	52.6°	85.1°	84.4°	58.3°
C3	54.1°	38.1°	60.0°	88.0°
C4	0.6°	6.0°	/	/
C5	34.1°	33.6°	57.3°	55.8°

[a]The two ψ angles in **C5** are averaged.

Table S3. Photophysical data for probes **C1~C5** and their CN^- adducts formed upon addition of 3 eq. CN^- in dichloromethane.

entry	τ_1, ns	τ_2, ns
C1	4.34	9.66
C1-CN	4.36	/
C2	3.77	12.04
C2-CN	5.52	/
C3	5.40	17.98
C3-CN	21.33	/
C4	7.91	/
C4-CN	10.61	/
C5	0.55	6.12
C5-CN	6.44	/